Published in final edited form as:

*AJNR Am J Neuroradiol*. 2019 August ; 40(8): 1291–1298. doi:10.3174/ajnr.A6119.

# White matter lesion penumbra shows abnormalities on structural and physiologic MRI in the CARDIA cohort

**Ilya M. Nasrallah, MD, PhD**[1], **Meng-Kang Hsieh**[2], **Guray Erus, PhD**[2], **Harsha Battapady**[2], **Sudipto Dolui, PhD**[3], **John A. Detre, MD**[3], **Lenore J. Launer, PhD**[4], **David R. Jacobs, PhD**[5], **Christos Davatzikos, PhD**[2], **R. Nick Bryan, MD, PhD**[1]

[1]Department of Radiology, University of Pennsylvania, Philadelphia, PA

[2]Center for Biomedical Image Computing and Analytics, University of Pennsylvania, Philadelphia, PA

[3]Department of Neurology, University of Pennsylvania, Philadelphia, PA

[4]National Institute on Aging, National Institutes of Health, Bethesda, MD

[5]Division of Epidemiology, School of Public Health, University of Minnesota, Minneapolis, MN

## Abstract

**Background and purpose:** White matter lesions are one age-related manifestation of cerebrovascular disease, but sub-threshold abnormalities have been identified in non-lesional WM. We hypothesize that structural and physiologic MRI findings of early cerebrovascular disease can be measured in middle-aged subjects in tissue adjacent to WM lesions, termed penumbra.

**Methods:** WM lesions were defined using automated segmentation in 463 subjects, ages 43–56, from the Coronary Artery Risk Development in Young Adults (CARDIA) longitudinal observational cohort study. 0–2mm and 2–4mm thick spatially-defined penumbral WM tissue ROI were defined as rings surrounding WM lesions. Remaining WM was defined as distant normal-appearing WM (dNAWM). Mean signal intensities were measured for FLAIR, T1-, and T2-weighted images, and from fractional anisotropy, mean diffusivity, CBF, and vascular reactivity maps. Group comparisons were made using Kruskall-Wallis and pairwise t-tests.

**Results:** Lesion volumes averaged 0.738±0.842cm$^3$ (range 0.005–7.27cm$^3$). Mean signal intensity for FLAIR, T2, and mean diffusivity were increased while T1, fractional anisotropy, and CBF were decreased in WML versus distant normal-appearing WM, with penumbral tissues showing graded intermediate values (corrected $p<0.001$ for all group/parameter comparisons). Vascular reactivity was significantly elevated in WML and penumbral tissue compared to dNAWM (corrected $p\leq0.001$).

**Conclusion:** Even in relatively healthy 43–56-year old subjects with small WML burden, structural and functional MRI in penumbral tissue reveal significant signal abnormalities versus

Corresponding Author: Ilya M Nasrallah, MD, PhD, Department of Radiology, University of Pennsyvlania, 3400 Spruce Street, Philadelphia, PA 19104, Phone: (215) 615-8054, Fax: (215) 349-5843, ilya.nasrallah@uphs.upenn.edu.

This data was in part presented in part at the 2016 ASNR Annual Meeting in Washington, DC.

WML and other normal WM. Findings suggest that WM injury onset starts by middle age and involves substantially more tissue than evident from focal WML visualized on structural imaging.

## Introduction

Cerebral white matter lesions (WML), or leukoaraiosis, are common age-related MRI findings but may be present in younger individuals[1]. WML are associated with cognitive decline[2–4], future infarction, depression[5] and poor clinical prognosis[6]. WML commonly affect terminal vascular territories and burden progresses[7] by expansion of existing lesions and development of new lesions.

Pathologically, WML demonstrate capillary loss, arterial tortuosity, gliosis[8], demyelination and ischemia[9]. Imaging has shown physiological abnormalities in WML, including cerebral blood flow (CBF)[10, 11] and vascular reactivity (VR)[12] decreases and increased blood-brain barrier permeability[13]; other studies have established that age, hypertension and smoking are important risk factors for WML[14]. These observations lead to the hypothesis that cardiovascular risk factors result in chronic vascular impairment that cause tissue damage visualized as WML, although there is also evidence for progression through acute injury[15]. Together, these injuries likely interfere with axonal function and connectivity, contributing to clinical deficits, including cognitive decline.

Many methods exist to automatically segment WML from MRI, usually relying on structural MRI signal intensity characteristics. Since WML are usually progressive, MRI techniques sensitive to early pathologic changes may identify at risk tissue in normal-appearing white matter (NAWM). Indeed, MRI studies, mostly in elderly populations[7, 16, 17], have demonstrated abnormalities in several measurements of NAWM on conventional MRI. NAWM near WML is most likely to show abnormality[17]. One large study evaluating signal abnormalities in NAWM found increased FLAIR signal, increased mean diffusivity (MD), and decreased fractional anisotropy (FA) in tissue that ultimately developed into WML[7] while a smaller study showed similar findings for low CBF[18]. White matter integrity metrics from diffusion tensor imaging, like FA and MD, are also abnormal in NAWM in people with WML[19–21]. However, many previous studies are limited by small sample sizes and region of interest image analysis techniques that do not broadly evaluate WML and NAWM. Furthermore, structural, diffusion, and physiological parameters have not been simultaneously evaluated in WML versus NAWM to allow evaluation of correlations between MRI parameters, which might be redundant due to measurement of similar physiology or for technical reasons.

We hypothesize that even in the relatively healthy CARDIA cohort, aged 43–56, visible WML underrepresent total white matter abnormality. Evidence of more widespread injury may suggest that antihypertensive therapy and other therapies to control vascular risk factors may benefit brain health starting in middle age. We investigated tissue immediately surrounding WML, termed WML penumbra, which was likely exposed to similar vascular stressors, predicting that the imaging correlates of injury would be intermediate between WML and distant NAWM. We simultaneously characterized structural abnormalities,

measures of white matter integrity, and vascular physiological parameters to determine the characteristics of WML penumbral tissue using MRI.

## Methods

### Study sample

The Coronary Artery Risk Development in Young Adults (CARDIA) study is a prospective, longitudinal cohort study evaluating the development of vascular risk factors in healthy young adults, who provided informed consent to participate. The original cohort consisted of 5,115 healthy black and white participants, aged 18–30[22]. In the 25th year of follow-up (Y25), at mean age of 50 years old, brain MRI was performed between 8/19/2010 and 8/31/2011 in 719 randomly-selected CARDIA subjects who had no contraindications to MRI. Structural (T1, T2, FLAIR), diffusion (MD, FA), and physiological data (ASL perfusion, breath-hold fMRI) were acquired and complete, analyzable data sets were obtained in 463 subjects (Supplemental Figure 1) from two sites: University of Minnesota (UMN, n=250) and Kaiser-Permanente Division of Research (KPDR, n=213), both using 3T Siemens TimTrio scanners. Demographic composition of this subgroup is shown in the Table 1; these are similar to the overall CARDIA Y25 MRI cohort[1] and there was no significant difference based on site except for significantly higher Body Mass Index (BMI) at the UMN site.

### MRI imaging and analysis

This study is a retrospective analysis of prospectively acquired data, approved by the institutional review board of the University of Pennsylvania. The CARDIA brain MRI protocol has been published previously[1]; briefly, it included T1 (TR=1900, TE=2.89, FOV=250mm, thickness=1mm, slices=176, native resolution=1mm isotropic), T2 (TR=3200ms, TE=409ms FOV=250mm, thickness=1mm, slices=176, native resolution=1mm isotropic), FLAIR (TR=6000ms, TE=285ms, FOV=258mm, thickness=1mm, slices=160, native resolution=1mm isotropic), 30-direction diffusiontensor imaging (TR=7400ms, TE=82ms, FOV=246mm, thickness=2.2mm, slices=64, native resolution=2.2mm isotropic), pseudocontinuous arterial spin label (pcASL) perfusion (TR=4000, TE=11, FOV=220 mm, thickness=5mm, slices=20, native resolution=3.4 × 3.4 × 6mm), and breath-hold blood oxygen level dependent (BOLD) functional MRI (fMRI, TR=2000ms, TE=25ms, FOV=224mm, thickness=3.5mm, slices=35, native resolution=3.5mm isotropic). Scanner performance was monitored with quarterly ADNI and fBIRN phantom acquisition, with the scanners showing stability of phantom measurements throughout the study.

Processing of structural MRI sequences first involved histogram normalization and bias field correction of raw image data, which improves comparability of the uncalibrated, ordinal data, followed by template registration[23] and semi-automated tissue segmentation[24]. WML segmentation was performed using a previously validated supervised learning-based multi-modal segmentation method[24, 25]. This support vector machine classifier was originally trained on multi-modal MRI data from a separate training set with expert human manual segmentation of WML. It provides segmentation based on structural MRI (T1, T2, FLAIR)

that strongly correlated with a human observer definition of WML in the training set. The model was applied on CARDIA subjects to calculate binary WML masks, and has been used in prior analyses of CARDIA imaging data. WML masks were morphologically dilated to define 2mm rims of adjacent penumbra tissue (0–2mm and 2–4mm) within tissue classified as NAWM. These 2mm ROIs were selected based on a compromise between the intrinsic spatial resolution of the acquired data and relatively narrow expected transition from WML to normal tissue. Voxels within these penumbra ROI are more likely to have been exposed to similar vascular injury compared to those in WML and therefore more likely to be abnormal, however there is no a priori standard for sub-classifying these voxels. Distant normal-appearing white matter (dNAWM) was defined by eroding the white matter segmentation mask from the GM and WML/penumbra ROIs by 2mm to avoid partial volume effects.

From DTI, FA and MD scalar maps were calculated. CBF maps were calculated from pcASL[26]. Maps of vascular reactivity (VR) as measured by percent signal-change in BOLD fMRI between breath-hold and rest states were generated using a method similar to Murphy et al.[27]. To summarize, breath holding was used to elevate blood $CO_2$ and thereby induce cerebral vasodilation to effect changes in BOLD signal. During acquisition of the BOLD fMRI, subjects were cued to follow four 16-second breath holds using E-Prime (Psychology Software Tools, Inc, Sharpsburg, USA). Using FSL, the resulting images were motion corrected and smoothed and a whole-brain generalized linear model (GLM) analysis was performed using a 9 second delay to account for hemodynamic lag. We excluded subjects without activation of the superior sagittal sinus (SSS), a marker of breath hold compliance, measured as Z-score within the SSS<2.3. VR Z-score maps were thresholded at Z>2.3 and percent activation calculated relative to the median Z-score in the SSS. Only voxels with activation above this threshold were included for analysis. Maps for FA, MD, CBF, and VR were registered to T1 space and interpolated to 1mm isotropic resolution.

3D volumes and imaging maps were aligned using FSL (http://www.fmrib.ox.ac.uk/fsl/). In each of the four ROIs – WML, 0–2mm penumbra, 2–4mm penumbra, and dNAWM (Figure 1) – mean intensity was extracted from each of the acquired sequences, resulting in mean intensity values for each of the four regions for FLAIR, T1, T2, FA, MD, CBF, and VR. For VR, to evaluate the possible significant contributions of noise from subjects with few activated voxels, analyses were repeated after exclusion of subjects with the lowest quartile of activated voxels for each ROI as a secondary analysis.

## Statistics

Statistical analysis was performed using Python 2.7. Mean values for each parameter were compared between groups using Kruskal-Wallis and Wilcoxon signed-rank pairwise t-tests. Regression analysis of median intensity across regions was performed by applying a generalized estimating equation to Z-score normalized intensity measures. Correlation matrices using Pearson product-moment correlation coefficients were computed for intensities of each parameter. Holm-Bonferroni correction was used to adjust for multiple comparisons in pairwise t-tests and correlation matrices. Recursive feature elimination with stratified 10-fold cross-validation (RFECV) was performed to determine the optimal set of parameters that best predicted assignment to WML, 0–2mm penumbra, 2–4mm penumbra,

and NAWM ROIs for each voxel. This method initially used all parameters to train the estimator, and then features with the lowest weights were recursively eliminated until further feature removal reduced classification accuracy. We investigated the associations of imaging parameters in WML and penumbras with clinical risk factors of systolic blood pressure (SBP), BMI, smoking status, and sedentary behavior, as previously defined[1], controlling for imaging site and demographic factors of age, gender, and race using ordinary least square linear regression modeling with Z-score transformed data, adjusting for age, sex, race, and site. Similarly, we evaluated overall cardiovascular risk using a derived risk factor score ($RF_{score}$, range 0–6) that was generated for each participant as a count of which of the following six risk factors were present: hypertension (SBP > 140 or on antihypertensive medication), hypercholesterolemia (total serum cholesterol >100 or on cholesterol medication), sedentary behavior (>75$^{th}$ percentile, equivalent to >8.5 hours of sedentary behavior per day), diabetes (if present), BMI (if ≥30), or history of smoking (current and former smokers).

## Results

WML volumes averaged 0.738±0.842cm$^3$ (range 0.005–7.27cm$^3$) in the 463 subjects from the CARDIA Y25 cohort included in this study. Derived volumes of 0–2mm penumbra, 2–4mm penumbra, and dNAWM measured 2.78±2.26 cm$^3$, 5.81±4.21 cm$^3$, 219±36.8 cm$^3$, respectively.

We found significant differences for most parameters across ROI (Table 2, Figure 2). Mean FLAIR intensity, T2 and MD were higher in WML than dNAWM while mean T1 intensity, FA, CBF were lower (all $p<0.001$). For all these parameters, penumbra tissue showed intermediate values that were significantly different from each other and from both WML and dNAWM ($p<0.001$ for all pairwise t-tests). Regression analysis by group demonstrated a strong effect of tissue type on signal intensities for FLAIR, T1, T2, MD, and FA, all statistically significant ($p<0.001$), with the strongest effects seen for structural parameters (Table 2); these correlations were not significantly affected by adjusting for site. There was no association between intensity values and subject age for any ROI (data not shown).

VR calculated from breath-hold fMRI showed lower mean number of activated voxels in WM versus GM (67.0±27.9% versus 78.3 ±29.5% showed activation, respectively, $p<0.001$). Activated voxels in the WM also showed lower percent signal change compared to GM (0.86±0.40% vs. 1.43±0.57%, $p<0.001$). Compared to prior studies with 5% $CO_2$ inhalation, which achieves more reproducible blood $CO_2$ levels, our VR results showed similar values of WM percent activation[28] and ratio between GM and WM activation[29]. However, the VR data is less reliable than other measures, as values are not available for all voxels especially in WML (Supplemental Table 1), and are more variable.

Compared to dNAWM, mean VR was significantly higher in WML ($p=0.001$) and penumbral regions ($p<0.001$, Table 2, Figure 2, Supplemental Figure 2). Since only a subset of voxels within a region show measurable activation to contribute to VR signal, variability in mean VR measures was high in subjects with small lesion volumes, probably due to noise. Repeating the comparison but excluding 117 subjects in the lowest quartile of lesion

volumes showed a decrease in mean WML VR from 0.78±0.49 to 0.75±0.38 with reduction in variability, but the relationships to the other regions remained similar.

We investigated the correlations between the six parameters to evaluate whether some of these variables provided redundant information (Figure 3). There were few consistent relationships between variables and most correlations were low. MD showed the most stable correlations to other parameters across regions, but these correlations were moderate at best. Strong correlations were seen only with the positive correlation of T1 and FLAIR in dNAWM and overall and with negative correlation between T1 and T2 in WML and penumbras; however both of these relationships were weak or reversed in the other regions. CBF and VR were weakly correlated with other variables. Overall correlations were dominated by dNAWM, which had the largest volumes. The variability of magnitude and direction of the correlations between parameters suggest that these parameters provide unique information that may be useful for characterizing abnormal white matter tissue. To investigate which features are most useful for classification of voxels into the WML, penumbral, and NAWM ROI, we employed recursive feature elimination[30]. This process determined that T1, FLAIR, and T2 provided optimal classification of voxels to these ROI. MD was the next most relevant but was not selected, followed by FA, CBF and VR. The cross validation accuracy versus number of features selected is shown in Supplemental Figure 3.

Finally, we evaluated relationships of signal intensities for FLAIR and FA, as representative structural and DTI measures, as well as CBF, and VR in WML and penumbral tissue with vascular risk factors. As expected, we found significant associations of higher WML volume with higher SBP ($p<0.001$), even without correcting for antihypertensive therapy, and with $RF_{score}$ ($p<0.001$). In multivariate modeling of regional intensities adjusting for age, race, sex, and site, $RF_{score}$ showed significant association only with mean CBF in the WML and both penumbral ROI (Supplemental Table 2), with higher $RF_{score}$ associated with lower mean CBF. Next, we looked at a model with the same demographic factors but including hypertension, hypercholesterolemia, smoking history, diabetes, sedentary behavior, and BMI as independent variables, instead of the risk score (Supplemental Table 3). Sedentary behavior was associated with significant differences in mean T1 and mean T2 within WML and with VR in the 2–4mm penumbra. Smoking history was associated with significant differences in CBF and VR within lesions and with T1 and MD in both penumbras. BMI was inversely associated with CBF across all 3 regions. Other risk factors did not show significant associations in these models.

## Discussion

While WML usually appear as discrete lesions, prior studies in elderly populations found associations with abnormality in other, visually normal WM tissue. Although strongly associated with age and hypertension, WML are seen in young, normotensive individuals. We examined MRI characteristics in WML and penumbra in adults aged 43–56 in the CARDIA study. The CARDIA brain MRI cohort has much lower mean age and WML volume compared to most other studies that have evaluated WML and penumbra; for comparison, the study of de Groot et al. had a mean age of 67 years with median WML

volume of 3.4 $cm^3$ [7], WHIMS, which used the same WML classifier method as this current study, had a mean age of 78.5 years and mean WML volume of 4.3 $cm^3$ [31], and that of Promjunyakul et al. had a mean age of 85 years with mean WML volume of 11.2 $cm^3$ [16]. Most CARDIA MRI participants were normotensive (57%), with 11% prehypertensive and 32% hypertensive[1].

Despite low lesion burden, we found statistically significant abnormalities in all measured structural, diffusion, and physiologic MRI parameters in penumbral tissue, encompassing on average more than 10-fold larger volume than WML (Figure 2, Table 2). Signal abnormalities in WML and penumbral regions were worsened when vascular risk factors were present, specifically with relationships between SBP and FLAIR intensity and between SBP and BMI and CBF. These findings indicate that, as in the elderly, WM damage is more extensive in middle age than represented by the typical low WML volume, suggesting that early intervention on reversible cardiovascular risk factors may yield benefit in slowing progression of this damage. Recent results from the SPRINT trial has shown that aggressive blood pressure control may slow progression of WML volume[32], and it is possible that such intervention would also affect penumbral tissue. Interestingly, we did not find an association between regional signal intensities and age, which has been shown to be the strongest risk factor for WML in prior studies. It is possible that at the younger age of this cohort, lesions are primarily the consequence of hypertension, and therefore growth could potentially be prevented with adequate antihypertensive therapy. Overall, we found limited associations between cardiovascular risk factors and regional intensity values, however effects were shown in multivariate analyses between a cumulative risk factor score and individually with sedentary behavior, smoking history, and BMI. These associations require further investigation, particularly as the exposure lengthens with aging.

The physiological MRI variables, CBF and VR, have been less extensively studied in WML and penumbra. Our study confirms prior reports showing decreased CBF in WML[10, 11] and penumbra compared to NAWM[16]. Unlike the other imaging parameters, which probably measure sequelae from injury, CBF and VR may more directly measure etiologic abnormalities for WML; interestingly this was the only variable significantly associated with the number of cardiovascular risk factors. Regional differences were less pronounced in the physiological CBF and VR data, partially related to lower signal to noise and resolution and greater biological variability. Compared to VR, CBF is more technologically mature with greater potential for widespread implementation.

The few studies that have evaluated VR in WML mostly evaluated global VR, which is dominated by GM, and more often used transcranial Doppler ultrasound rather than MRI. Hypertension and vascular risk factors have been associated with decreased VR; some but not all studies showed adverse associations of global cerebral VR with WML[33–35]. Studies in elderly subjects measuring BOLD VR with a more reproducible $CO_2$ inhalation method showed 50–60% decreased VR in WML versus NAWM[12, 28]. In our study, mean VR was unexpectedly higher in WML and penumbras than dNAWM; if validated this might suggest a difference in physiology in WML and at-risk tissue in younger or low-WML volume subjects compared to elderly or high WML volume subjects. Increased VR may indicate a

compensatory, possibly protective, vasoreactivity versus an indication of intrinsic, possibly harmful, abnormality of the vessels.

The mechanisms behind WML propagation are unknown. Vascular compromise may spread from extant WML or independent events may accumulate in vulnerable territory. We found that adjacent tissue, including 2–4mm removed from WML, showed detectable abnormalities on structural imaging, measures of white matter integrity, and physiological parameters. For all parameters except VR, penumbra showed intermediate values transitioning between WML and dNAWM, suggesting lesser injury. Longitudinal evaluation comparing regions that develop into lesions versus those that do not will likely identify heterogeneity within penumbral tissue and show whether these parameters can predict lesion growth. Unfortunately, prospective prediction of lesion development has not yet been successful. Scoring each voxel based on a combination of MR parameters may provide a means to identify at-risk regions. We found that a combination of FLAIR, T1, and T2 provided optimal, non-redundant classification of voxels into the WML, penumbral, and dNAWM ROI, however it remains to be seen whether longitudinal change in WML is better predicted by baseline structural or physiological measures or a combination.

There are several limitations of this study. Due to lower resolution of diffusion and functional sequences compared to structural imaging, partial volume effects likely affect calculation of mean intensities. However, significant differences were seen between WML and the 2–4mm penumbra, which would be less affected by partial volume effects from WML. The WML segmentation classifier used to identify WML is conservative, and as a result some tiny WML may be included in other regions, which should decrease statistical differences by increasing variability. Using two, 2-mm concentric penumbral rings was a compromise between the need to evaluate a relatively narrow band of tissue around WML and the need to reduce partial volume effects. Others have shown similar gradated changes extending even further around WML[16]. The morphologic dilation used to generate the penumbral ROI overlooks expected heterogeneity of penumbral tissue, however mixing tissues with varying levels of injury in concentric ROIs is expected to decrease power of this study. T1, T2, and FLAIR intensities vary depending on scanner and imaging parameters. Our data was acquired on the same scanner model with the same imaging parameters and normalization techniques were implemented to harmonize the data, however this affects generalizability to other sites. We made no correction for the mild, normal regional variations of signal intensity in the brain, which has been previously performed[7]. Normal signal variations may accentuate some regional differences; for example FLAIR is normally slightly increased in periventricular regions most commonly affected by WML relative to NAWM. FA, however, shows significant decreases in regions that normally have higher FA, suggesting that applying regional intensity corrections might result in even greater differences.

## Conclusions

Even in relatively healthy, middle-aged adults with low total WML burden, WMLs have a substantial penumbra of tissue with abnormalities quantifiable by structural and physiological MRI parameters, in some individuals involving volumes over ten times larger

than WML visible on FLAIR. Further, the gradation of signal abnormalities in penumbra tissue suggests early/milder injury, compatible with the hypothesis that injury expands from established lesions; this penumbral tissue may be a target for therapeutic intervention to prevent worsening of WML. Multimodal MRI imaging may better define injured white matter than methods that use only structural data. Further investigation is needed to determine the optimal combination of parameters to prospectively identify the full extent of abnormal white matter and the effects of these abnormalities on neural circuits and cognition. An epidemiologic priority is to examine whether the volume and characteristics of these expanded injury regions predicts future lesions and risk of brain-related disease.

## Supplementary Material

Refer to Web version on PubMed Central for supplementary material.

## Acknowledgements:

The Coronary Artery Risk Development in Young Adults Study (CARDIA) is conducted and supported by the National Heart, Lung, and Blood Institute (NHLBI) in collaboration with the University of Alabama at Birmingham (HHSN268201300025C & HHSN268201300026C), Northwestern University (HHSN268201300027C), University of Minnesota (HHSN268201300028C), Kaiser Foundation Research Institute (HHSN268201300029C), and Johns Hopkins University School of Medicine (HHSN268200900041C). CARDIA is also partially supported by the Intramural Research Program of the National Institute on Aging (NIA) and an intra-agency agreement between NIA and NHLBI (AG0005). This manuscript has been reviewed by CARDIA for scientific content.

The authors thank Raymond Pomponio for statistical assistance.

## Abbreviations:

| | |
|---|---|
| **WML** | White matter lesion |
| **dNAWM** | distant normal-appearing white matter |
| **FA** | fractional anisotropy |
| **MD** | mean diffusivity |
| **VR** | vascular reactivity |
| **SBP** | systolic blood pressure |
| **BMI** | Body Mass Index |

## References:

1. Launer LJ, Lewis CE, Schreiner PJ, et al. Vascular Factors and Multiple Measures of Early Brain Health: CARDIA Brain MRI Study. PLoS One 2015;10:e0122138 [PubMed: 25812012]
2. Jokinen H, Kalska H, Ylikoski R, et al. Longitudinal cognitive decline in subcortical ischemic vascular disease--the LADIS Study. Cerebrovasc Dis 2009;27:384–391 [PubMed: 19276621]
3. Verdelho A, Madureira S, Moleiro C, et al. White matter changes and diabetes predict cognitive decline in the elderly: the LADIS study. Neurology 2010;75:160–167 [PubMed: 20625169]
4. Debette S, Markus HS. The clinical importance of white matter hyperintensities on brain magnetic resonance imaging: systematic review and meta-analysis. Bmj 2010;341:c3666 [PubMed: 20660506]

5. Teodorczuk A, Firbank MJ, Pantoni L, et al. Relationship between baseline white-matter changes and development of late-life depressive symptoms: 3-year results from the LADIS study. Psychol Med 2010;40:603–610 [PubMed: 19671212]
6. Inzitari D, Pracucci G, Poggesi A, et al. Changes in white matter as determinant of global functional decline in older independent outpatients: three year follow-up of LADIS (leukoaraiosis and disability) study cohort. Bmj 2009;339:b2477 [PubMed: 19581317]
7. de Groot M, Verhaaren BF, de Boer R, et al. Changes in normal-appearing white matter precede development of white matter lesions. Stroke 2013;44:1037–1042 [PubMed: 23429507]
8. Brown WR, Thore CR. Review: cerebral microvascular pathology in ageing and neurodegeneration. Neuropathol Appl Neurobiol 2011;37:56–74 [PubMed: 20946471]
9. Fazekas F, Kleinert R, Offenbacher H, et al. Pathologic correlates of incidental MRI white matter signal hyperintensities. Neurology 1993;43:1683–1689 [PubMed: 8414012]
10. O'Sullivan M, Lythgoe DJ, Pereira AC, et al. Patterns of cerebral blood flow reduction in patients with ischemic leukoaraiosis. Neurology 2002;59:321–326 [PubMed: 12177363]
11. Brickman AM, Zahra A, Muraskin J, et al. Reduction in cerebral blood flow in areas appearing as white matter hyperintensities on magnetic resonance imaging. Psychiatry Res 2009;172:117–120 [PubMed: 19324534]
12. Sam K, Crawley AP, Poublanc J, et al. Vascular Dysfunction in Leukoaraiosis. AJNR Am J Neuroradiol 2016
13. Topakian R, Barrick TR, Howe FA, et al. Blood-brain barrier permeability is increased in normal-appearing white matter in patients with lacunar stroke and leucoaraiosis. J Neurol Neurosurg Psychiatry 2010;81:192–197 [PubMed: 19710048]
14. Grueter BE, Schulz UG. Age-related cerebral white matter disease (leukoaraiosis): a review. Postgrad Med J 2012;88:79–87 [PubMed: 22184252]
15. Conklin J, Silver FL, Mikulis DJ, et al. Are acute infarcts the cause of leukoaraiosis? Brain mapping for 16 consecutive weeks. Ann Neurol 2014;76:899–904 [PubMed: 25283088]
16. Promjunyakul N, Lahna D, Kaye JA, et al. Characterizing the white matter hyperintensity penumbra with cerebral blood flow measures. NeuroImage: Clinical 2015;8:224–229 [PubMed: 26106546]
17. Maniega SM, Valdes Hernandez MC, Clayden JD, et al. White matter hyperintensities and normal-appearing white matter integrity in the aging brain. Neurobiol Aging 2015;36:909–918 [PubMed: 25457555]
18. Bernbaum M, Menon BK, Fick G, et al. Reduced blood flow in normal white matter predicts development of leukoaraiosis. J Cereb Blood Flow Metab 2015;35:1610–1615 [PubMed: 25966951]
19. Schmidt R, Ropele S, Ferro J, et al. Diffusion-weighted imaging and cognition in the leukoariosis and disability in the elderly study. Stroke 2010;41:e402–408 [PubMed: 20203319]
20. Pelletier A, Periot O, Dilharreguy B, et al. Age-Related Modifications of Diffusion Tensor Imaging Parameters and White Matter Hyperintensities as Inter-Dependent Processes. Front Aging Neurosci 2015;7:255 [PubMed: 26834625]
21. Maillard P, Carmichael O, Harvey D, et al. FLAIR and diffusion MRI signals are independent predictors of white matter hyperintensities. AJNR Am J Neuroradiol 2013;34:54–61 [PubMed: 22700749]
22. Friedman GD, Cutter GR, Donahue RP, et al. CARDIA: study design, recruitment, and some characteristics of the examined subjects. J Clin Epidemiol 1988;41:1105–1116 [PubMed: 3204420]
23. Shen D, Davatzikos C. HAMMER: hierarchical attribute matching mechanism for elastic registration. IEEE Trans Med Imaging 2002;21:1421–1439 [PubMed: 12575879]
24. Zacharaki EI, Kanterakis S, Bryan RN, et al. Measuring brain lesion progression with a supervised tissue classification system. Med Image Comput Comput Assist Interv 2008;11:620–627 [PubMed: 18979798]
25. Lao Z, Shen D, Liu D, et al. Computer-assisted segmentation of white matter lesions in 3D MR images using support vector machine. Acad Radiol 2008;15:300–313 [PubMed: 18280928]

26. Wang Z, Aguirre GK, Rao H, et al. Empirical optimization of ASL data analysis using an ASL data processing toolbox: ASLtbx. Magn Reson Imaging 2008;26:261–269 [PubMed: 17826940]
27. Murphy K, Harris AD, Wise RG. Robustly measuring vascular reactivity differences with breath-hold: normalising stimulus-evoked and resting state BOLD fMRI data. Neuroimage 2011;54:369–379 [PubMed: 20682354]
28. Uh J, Yezhuvath U, Cheng Y, et al. In vivo vascular hallmarks of diffuse leukoaraiosis. J Magn Reson Imaging 2010;32:184–190 [PubMed: 20578025]
29. Reich T, Rusinek H. Cerebral cortical and white matter reactivity to carbon dioxide. Stroke 1989;20:453–457 [PubMed: 2494780]
30. Guyon I, Weston J, Barnhill S, et al. Gene selection for cancer classification using support vector machines. Mach Learn 2002;46:389–422
31. Kuller LH, Margolis KL, Gaussoin SA, et al. Relationship of hypertension, blood pressure, and blood pressure control with white matter abnormalities in the Women's Health Initiative Memory Study (WHIMS)-MRI trial. J Clin Hypertens (Greenwich) 2010;12:203–212 [PubMed: 20433539]
32. SPRINT Investigators. A Randomized Trial of Intensive Versus Standard Systolic Blood Pressure Control and Brain Structure: SPRINT MIND MRI *AAIC*. Chicago, USA; 2018
33. Matsushita K, Kuriyama Y, Nagatsuka K, et al. Periventricular white matter lucency and cerebral blood flow autoregulation in hypertensive patients. Hypertension 1994;23:565–568 [PubMed: 8175162]
34. Bakker SL, de Leeuw FE, de Groot JC, et al. Cerebral vasomotor reactivity and cerebral white matter lesions in the elderly. Neurology 1999;52:578–583 [PubMed: 10025791]
35. Birns J, Jarosz J, Markus HS, et al. Cerebrovascular reactivity and dynamic autoregulation in ischaemic subcortical white matter disease. J Neurol Neurosurg Psychiatry 2009;80:1093–1098 [PubMed: 19535355]

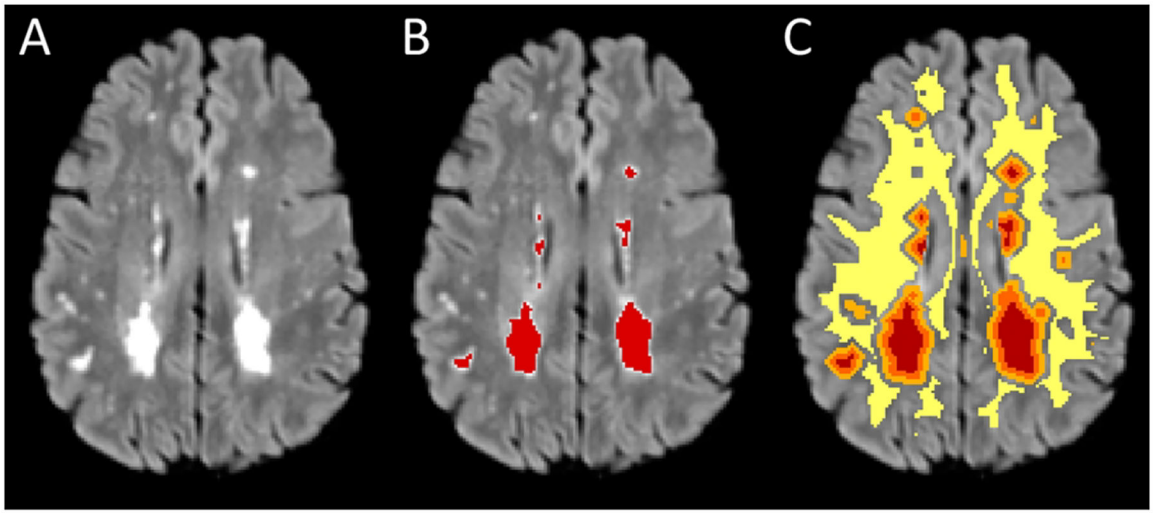


**Figure 1:**
Example FLAIR image showing (a) WML, (b) WML segmentation in red, (c) WML (red), 0–2mm (orange) and 2–4mm (light orange) penumbra, and dNAWM (yellow). dNAWM is eroded from GM to eliminate partial volume effects between these tissue types.

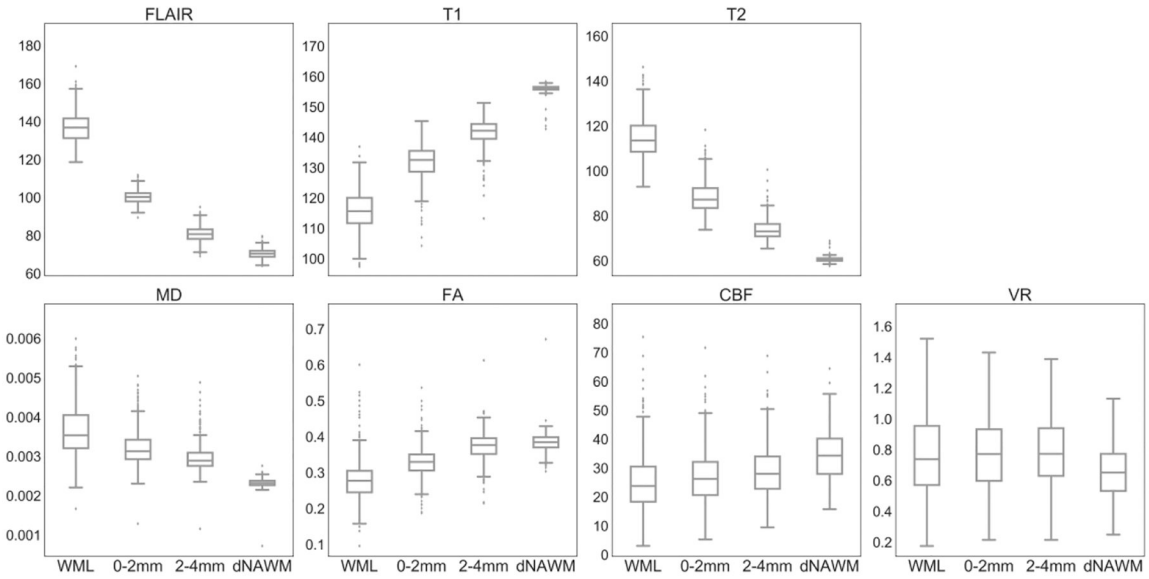


**Figure 2.**

Box plots of mean intensity values for each region. CBF is measured in $mm^3$/100gm/min and VR shows mean percent signal change. For vascular reactivity, outliers are excluded (comprising ~10% of the sample) to better demonstrate differences between means. Graph with outliers is available (supplemental figure 2). For each parameter, mean values are significantly different between all pairwise comparisons between ROIs with corrected $p<0.001$ except for VR where comparison of WML and dNAWM shows corrected $p=0.0013$ and where there is no significant difference among WML and the two penumbra regions ($p>0.4$).

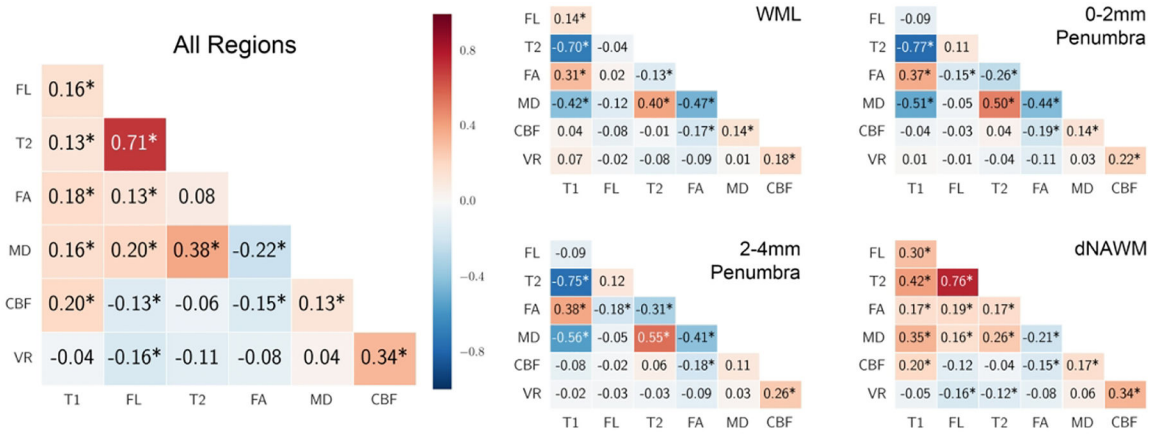


**Figure 3:**

Correlations between the seven MRI variables (Pearson's r). Correlation is shown for all voxels in all regions combined and separately for each region. Positive correlations are shaded red and negative correlations are shaded blue. * Bonferroni-Holm corrected $p<0.05$.

**Table 1:**

Demographic and risk factor data of the CARDIA MRI subjects included in this study.

| | **Total** | **KPDR** | **UMN** | **p value** |
|---|---|---|---|---|
| N | 463 | 213 | 250 | NA |
| Mean age (years) | 50.5 (+/− 3.4) | 50.5 (+/− 3.4) | 50.5 (+/− 3.3) | 0.98 |
| Race | Black 36% | 38% | 34% | 0.48 |
| | White 64% | 62% | 66% | |
| Gender | Male 47% | 47% | 46% | 0.98 |
| | Female 53% | 53% | 54% | |
| Mean BMI | 28.3 (±5.3) | 27.6 (± 5.4) | 28.9 (±5.2) | 0.009 |
| Mean Systolic/Diastolic blood pressure | 118 (±15) / 74 (±12) | 118 (±14) / 74 (±11) | 119 (±16) / 73 (±12) | 0.58/0.66 |
| Diabetic (%) | 7.6% | 6.9% | 8.2% | 0.61 |
| Smoking History | Never 60% | Never 67% | Never 53% | 0.005 |
| | Former 25% | Former 22% | Former 28% | |
| | Current 15% | Current 11% | Current 19% | |
| Sedentary behavior | >75$^{th}$ %ile 19% | >75$^{th}$ %ile 18% | >75$^{th}$ %ile 20% | 0.55 |
| Hypercholesterolemic | 69% | 71% | 68% | 0.38 |
| Mean Risk Factor Score (range 0–6) | 2.1 (± 1.3) | 1.9 (±1.2) | 2.2 (±1.3) | 0.06 |

**Table 2:**

Regional volumes and mean intensity values for the six MRI parameters with standard deviation in parentheses and 95% confidence intervals for intensity parameters in brackets. Kruskal-Wallis tests were significant for all parameters and pairwise comparisons had $p<0.001$ except WML and penumbral ROIs did not show significant differences in VR. Slope of linear regression across the four regions for intensity variables using median value is shown in the last column; regression analyses were all statistically significant with $p<0.001$.

| | WML | 0–2mm penumbra | 2–4mm penumbra | dNAWM | Regression Coefficient |
|---|---|---|---|---|---|
| Mean volume ($cm^3$) | 0.738 (0.842) | 2.78 (2.26) | 5.81 (4.21) | 219 (368) | NA |
| | [0.661, 0.815] | [2.57, 2.99] | [5.43, 6.19] | [186, 253] | |
| FLAIR intensity | 136 (10.1) | 98.9 (3.50) | 79.4 (3.71) | 70.8 (2.58) | −0.854 |
| | [135,137] | [98.6,99.2] | [79.1, 79.7] | [70.6, 71.0] | |
| T1 intensity | 116 (6.43) | 132 (5.80) | 142 (4.50) | 156 (1.31) | 0.824 |
| | [115,117] | [132,133] | [142, 142] | [156, 156] | |
| T2 intensity | 115 (8.62) | 88.3 (6.82) | 74.1 (4.75) | 60.6 (1.02) | −0.734 |
| | [114, 115] | [87.7, 88.9] | [73.7, 74.5] | [60.5, 60.7] | |
| FA | 0.279 (0.0554) | 0.328 (0.0411) | 0.374 (0.0380) | 0.384 (0.0254) | 0.630 |
| | [0.273, 0.284] | [0.324, 0.331] | [0.371, 0.377] | [0.382, 0.386] | |
| MD ($10^{-3}$) | 3.68 (0.662) | 3.23 (0.445) | 2.97 (0.344) | 2.33 (0.112) | −0.578 |
| | [3.62, 3.73] | [3.19, 3.27] | [2.93, 3.00] | [2.32, 2.34] | |
| CBF ($mm^3$/100gms/min) | 25.2 (10.3) | 26.9 (9.37) | 28.8 (9.06) | 34.4 (8.56) | 0.306 |
| | [24.3, 26.1] | [26.1, 27.7] | [28.0, 29.6] | [33.6, 35.2] | |
| VR (mean %change) | 0.776 (0.493) | 0.779 (0.379) | 0.790 (0.328) | 0.681 (0.377) | 0.192 |
| | [0.731, 0.821] | [0.745, 0.813] | [0.760, 0.820] | [0.647, 0.715] | |